Reversible Diels–Alder Reaction To Control Wrinkle Patterns: From Dynamic Chemistry to Dynamic Patterns

*Honghao Hou, Jie Yin, and Xuesong Jiang**

Surface patterns with periodic or random microarchitectures have become increasingly important for a broad range of applications because micro/nanoscale patterned topographies with spatial periodicity or aperiodicity endow materials with unique acoustic, electronic, optical, mechanical, and biological properties.[1–10] There is growing interest in creating hierarchical patterned surfaces that harness mechanical instabilities, especially surface wrinkles, due to their spontaneous nature, versatility, ability to generate large-area patterns, and tunability or even totally reversibility in response to various external stimuli.[5,11–16] The ability to tune complex pattern morphology that can possibly enable the on-demand control of the surface properties has attracted a great deal of attention because of the wide range of potential applications of such morphologies in enhanced and tunable optical devices,[11–14] responsive microfluidic channels,[11,15,16] flexible electronic devices,[14,17,18] and for switchable wettability,[12,15,19] smart adhesion,[12,16,20–23] and biomaterials.[24–26] Among numerous alternative processes for generating patterned surfaces,[5,6] surface wrinkles of a stiff skin on an elastomeric substrate were harnessed to create reversible patterns with on-demand tunable properties, which provided unique characteristics of surface morphology and properties with response to external stimuli.[11–23,27,28]

The wrinkles usually involve compressive stress that is caused by the modulus mismatch between the surface and the bulk of the materials and forms when the stiff-film/soft-substrate system is subjected to an in-plane compression ε that exceeds the critical strain threshold ε_C for inducing wrinkles.[29–34] According to linear buckling theory,[29,33,34] the characteristic amplitude (A) of the sinusoidal wrinkles can be predicted by minimizing the total energy of the system with respect to the surface modulus E, as in Equation (1):

$$\ln\left(A^2+h_t^2\right)=\frac{2}{3}\ln\overline{E}_f+\left(2\ln h_t+\ln 4\varepsilon-\frac{2}{3}\ln 3\overline{E}_s\right) \quad (1)$$

Here, the subscripts f and s refer to the top-layer film and substrate, respectively, h_t is the thickness of the top-layer skin film, $\overline{E}_f$ and $\overline{E}_s$ are the plane strain modulus for the top-layer film and substrate, respectively, and the Poisson's ratio of the top-layer film and polydimethylsiloxane (PDMS) substrate is 0.5. For a given thermally induced wrinkle system, the compressive stress can be estimated as $\varepsilon=\overline{E}_s\left(\partial_s-\partial_f\right)\Delta T/L$, where L is the substrate length, and ∂_s and ∂_f are the coefficients of linear thermal expansion for the film and substrate, respectively. If the parameters ε, h_t, and $\overline{E}_s$ are fixed, the modulus mismatch between the top-layer film ($\overline{E}_f$) and substrate ($\overline{E}_s$) is the only determining factor for the formulation and size of the wrinkles. Therefore, for the development of a reversible wrinkle system with smart adjustability from the smooth state to the wrinkle, it is crucial to precisely regulate the system-matched stress induced by the modulus mismatch through the desirable stimuli; for example, the wrinkle pattern can be tailored reversibly through externally imposed stimuli such as wetting and dewetting of the solvent,[11,12,20,21] and the release and stretch of prestrain.[14,17,18,26,27] Lu and co-workers reported an erasable wrinkle pattern on a PDMS substrate, in which the top azobenzene-containing polymer layer can be softened by light irradiation.[28] Although artificial physical intervention can be used to produce a tunable patterned surface with excellent properties, these methods of using an imposed stimulation ex situ are limited to discrete, special-purpose manual behaviors or require the alteration of the material's intrinsic properties. Because the modulus of polymer materials is usually related to the cross-linking density, according to Equation (1), it is possible to tune the morphology of the wrinkle pattern by controlling the modulus of the top layer, through the dynamic chemical cross-linking reaction.

Herein, we present a facile and effective strategy for the fabrication of a reversible wrinkle pattern with a morphology that can be dynamically erased and tuned in situ simply by controlling the dynamic Diels–Alder (D-A) chemical reaction (**Figure 1**). The D-A reaction between furan and maleimide was chosen due to its high reversibility and easy operability.[35–40] For temperatures from room temperature to approximately 100 °C, the cross-linked network with high modulus can be formed thorough the D-A reaction between furan and maleimide.[35–44] Meanwhile, the cross-linked D-A adducts can undergo a reverse reaction, which is known as a retro-D-A reaction, typically at temperatures above 120 °C, to reproduce the raw materials. The key point of this strategy is that the modulus of the top layer can be tuned by the dynamic D-A reaction cross-linking. The reversible nature of the D-A click chemistry enables a dynamic change of the pattern morphology from the smooth state to wrinkle pattern, which allows accurate control of the adhesion, wettability, and optical properties of the resulting surface. This one-step, robust approach for the fabrication of complex tunable wrinkle patterns provides the possibility to control surface properties on demand.

The strategy for the production of the reversible wrinkle pattern through the dynamic D-A reaction is illustrated in

Dr. H. H. Hou, Prof. J. Yin, Prof. X. Jiang
School of Chemistry & Chemical Engineering
State Key Laboratory for
Metal Matrix Composite Materials
Shanghai Jiao Tong University
Shanghai 200240, People's Republic of China
E-mail: ponygle@sjtu.edu.cn

DOI: 10.1002/adma.201602105

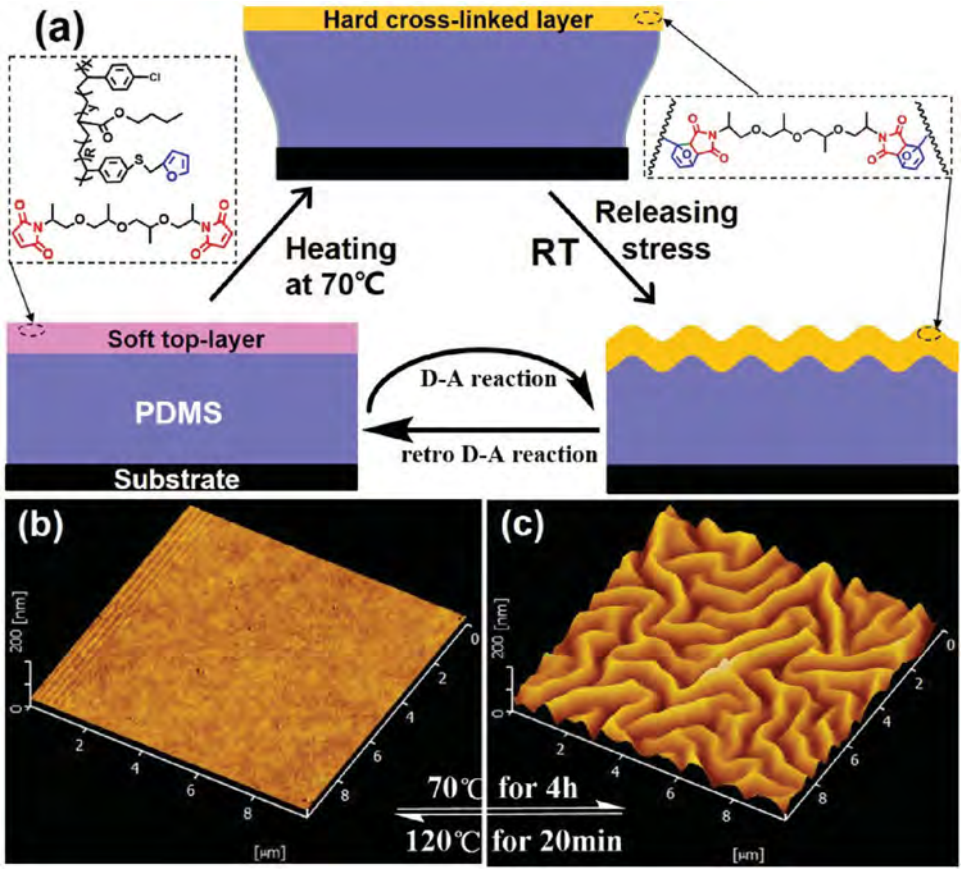

Figure 1. a) Strategy for a reversible wrinkle pattern based on a reversible Diels–Alder reaction; 3D AFM images demonstrating c) the generation and b) erasure of the reversible wrinkle pattern on the FBA/BMI coated film by the D-A reaction at 70 °C for 4 h, and the retro D-A reaction at 120 °C for 20 min. The thickness of the top layer is approximately 75 nm.

Figure 1a. A top layer comprised of furan-grated poly(butyl acrylate) (FBA) and bismaleimide (BMI) is coated onto the PDMS elastomer. A detailed description of the synthesis and characterization of the materials is in the Supporting Information (Figure S1–3). Upon heating to 70 °C for 4 h, the soft top layer of the FBA/BMI became rigid and cross-linked with a high modulus, due to the D-A reaction. Owing to the considerable mismatch in the modulus and thermal expansion ratio of the elastic PDMS substrate and the stiff cross-linked FBA/BMI top layer ($\partial_s \gg \partial_f$), an equi-biaxial compressive stress ε was generated upon cooling the bilayer to room temperature, which induced wrinkle formation as a result of releasing the localized stress to minimize the total energy of the system (Figure 1c).[33] After further heating to 120 °C for 20 min, the wrinkle pattern disappeared and the surface became smooth (Figure 1b)). This result should be ascribed to the retro-D-A reaction at the higher temperature, which causes the de-cross-linking of the FBA/BMI top layer. The soft and un-cross-linked top-layer cannot accumulate compressive stress, which results in the erasure of the wrinkle pattern. In contrast, our wrinkled surface induced by dynamic D-A cross-linking exhibits good long-term stability. Our as-prepared sample can be kept for more than one year at room temperature with no obvious change (Figure S4).

A series of control experiments was conducted to understand the effects of the surface modulus and D-A reaction on the wrinkle pattern. Instead of FBA/BMI, individual FBA or P(B-S-Cl)/BMI coated PDMS sheets underwent the same procedure of heating to 120 °C for 20 min. No obvious wrinkle pattern on the surface of either FBA or P(B-S-Cl)/BMI-coated PDMS was observed (Figure S5), which indicates that the D-A cross-linking procedure is necessary for the generation of the wrinkle pattern. Without D-A chemistry, the top layers of FBA or P(B-S-Cl)/BMI cannot be cross-linked, and their surface moduli are low. Thus the soft top layer cannot not restrain the localized stress after cooling to room temperature, and wrinkle pattern could not be generated. According to linear buckling theory, the wrinkle morphology is dependent on both the modulus and thickness of the FBA/BMI top layer. By controlling the thickness of the top-layer film via the variation of the spin-coating speed and the concentration of FBA/BMI (molar ratio = 1:1) solution, a series of wrinkle patterns was obtained after heating to 70 °C for 4 h (Figure S6). The characteristic A increased with increasing FBA/BMI thickness, which suggests that the wrinkle morphology can be tuned by tuning the thickness of the top layer.

To obtain detailed insights into the dependence of the wrinkle pattern on the D-A reaction, we traced the kinetics of the D-A reaction between BMI and FBA by ultraviolet–visible spectroscopy (UV–Vis) and real-time Fourier transform infrared spectroscopy (FT-IR). Upon heating to 70 °C, the intensity of

ADVANCED MATERIALS
www.advmat.de

www.MaterialsViews.com

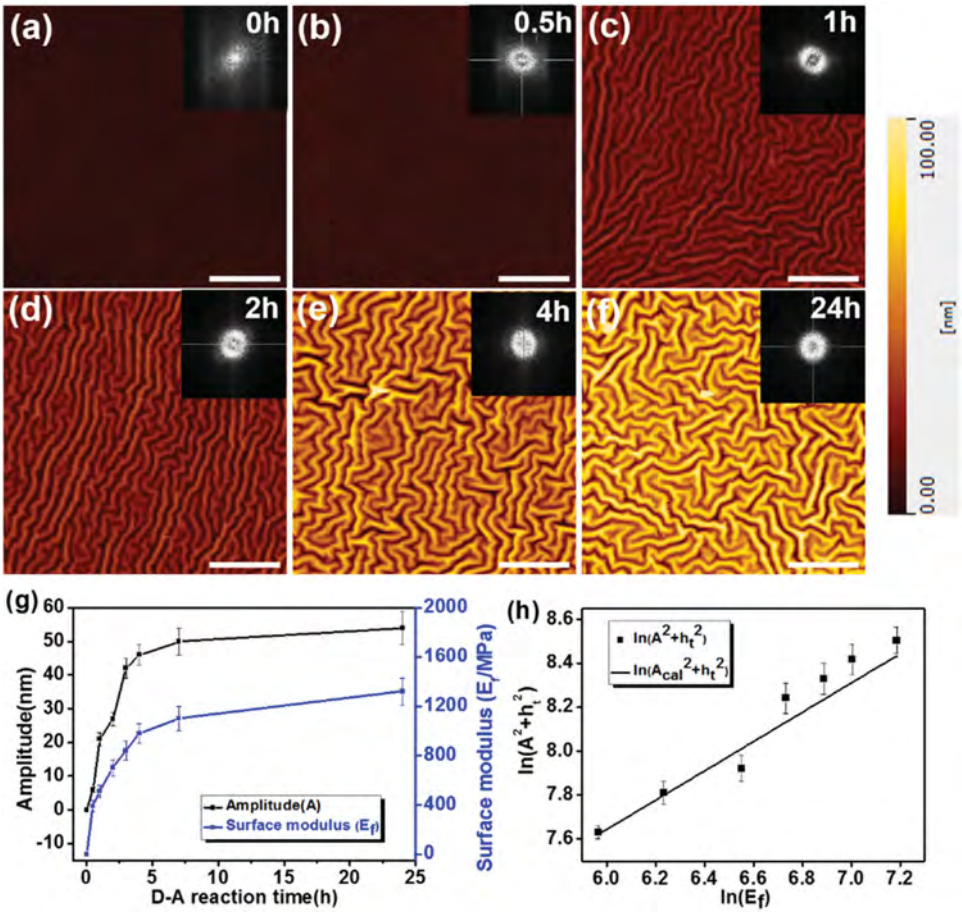

Figure 2. AFM images of the wrinkle pattern as a function of D-A reaction time at 70 °C: a) 0, b) 0.5, c) 1, d) 2, e) 4, and f) 24 h. The scale bar represents 5 μm, and the insets are the images that resulted from FFT of the corresponding AFM images. g) Amplitude A (black square, left vertical axis) and surface Young's modulus E_f (blue circle, right vertical axis) of the wrinkle patterned surfaces as a function of D-A reaction time. h) The experimental wrinkle amplitude (A, black square) and the theoretical wrinkle amplitude (A_{cal}, black line), predicted by Equation (2), of the wrinkle pattern as a function of surface modulus E_f. The thickness of the top layer is fixed at approximately 45 nm.

the characteristic "furan breathing" peak at 1209 cm^{-1}, which is typical for a D-A adduct,[40–44] increased gradually (Figure S7), while the UV characteristic absorption of BMI at approximately 219 nm decreased (Figure S8); this indicates the occurrence of a D-A reaction between the furan and maleimide rings. The degree of D-A reaction versus heating time, as determined by FT-IR and UV–Vis spectra, provided good qualitative online profiles of the D-A adducts' formation (Figure S8). Meanwhile, we observed the evolution of the wrinkle morphology dependence on D-A reaction time by using atomic force microscopy (AFM). As shown in **Figure 2**, a sequence of AFM images allows visualization of the reaction-time-dependent growth of the wrinkle pattern that is induced by the D-A reaction. The gradual progress of the D-A reaction results in a rapid increase of the wrinkle characteristic wavelength (λ) and amplitude (A) from the original smooth state to random wrinkles. After heating to 70 °C for 4 h, a wrinkling pattern with λ of 600 nm and A of 40 nm can be obtained. The growth of the microarchitecture can also be supported by the gradually increasing water contact angle (WCA) with increasing D-A reaction time, which will be discussed with the wettability of the wrinkled surface in the following section. At the beginning of the heating, the soft and un-cross-linked top-layer of FBA/BMI could not accumulate the compressive stress to trigger the surface mechanical instability, and the wrinkle pattern formation could not be generated. The wrinkle pattern should become obvious with increasing cross-linking density and surface modulus because the increasing compressive stress would exceed the threshold.

We believe that the D-A reaction leads to the cross-linked structure and enhances the modulus of the top layer, which results in the generation of wrinkles. To investigate the function of the surface moduli, the Young's modulus of the top layer, as determined by AFM force curves according to the Hertz model, was monitored during the progress of the D-A reaction (Figure 2g and Figure S9). The Young's modulus of the top layer increased dramatically from the initial value of 12 to 980 MPa, which was obtained after heating to 70 °C for 4 h. The gradually increased degree of cross-linking, combined with surface moduli, simultaneously results in a rapid increase of the wrinkle amplitude, which reaches a maximal value when the D-A reaction is completely finished. To elucidate the dependence of the wrinkling pattern on the modulus of the top layer, here we fixed the parameters for our wrinkle system at h_t = 45 nm, $\bar{E}_s$ = 2 MPa, L = 10 mm, ΔT = (70–25) °C = 45 °C,

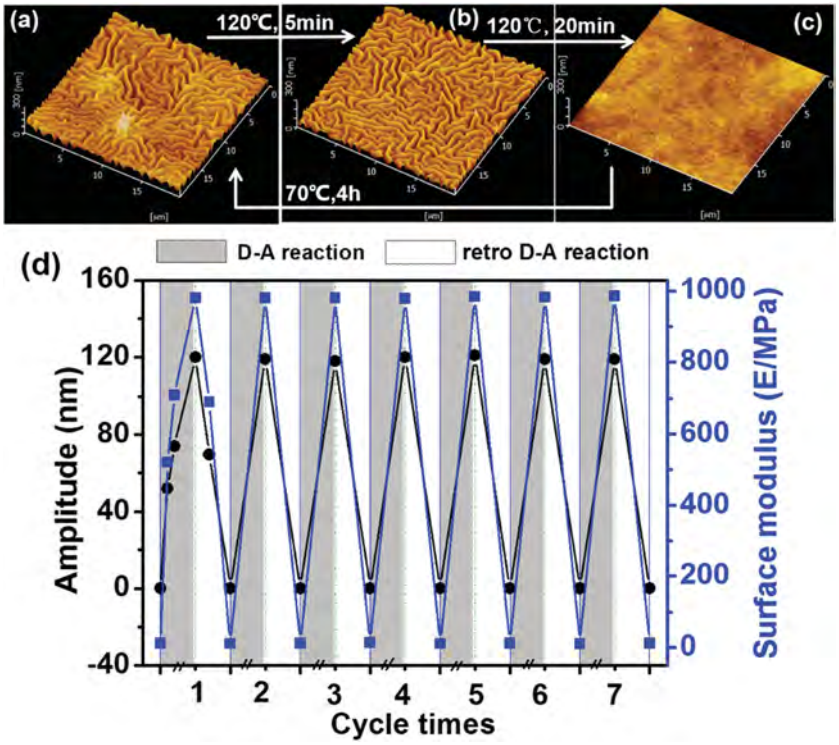

Figure 3. a–c) 3D AFM images and d) the evolution of their corresponding amplitude (*A*) and surface Young's modulus (*E*), showing the reversible morphology of the wrinkled surface with sequential, cyclic D-A reaction at 70 °C and subsequent retro-D-A reaction at 120 °C. d) The gray and white regions represent the D-A reaction heating to 70 °C for 4 h and the retro-D-A reaction heating at a higher temperature of 120 °C for 20 min, respectively. The thickness of the top layer is fixed at approximately 105 nm.

and $(\partial_s - \partial_f) \approx \partial_s = 300$ ppm °C^{-1} because the coefficient of thermal expansion of the PDMS sheet is far higher than that of the cross-linked FBA/BMI top layer, so that Equation (1) can be simplified to Equation (2), in which the wrinkle amplitude A (nm) can be calculated and predicted from the surface modulus $\overline{E}_f$ (MPa).

$$\ln\left(A^2 + 2025\right) = \frac{2}{3}\ln \overline{E}_f + 22.6138 \quad (2)$$

As depicted in Figure 2h, the values of both the experimentally measured statistical A and the theoretical A_{cal} increase with increasing Young's modulus of the top layer as the D-A reaction proceeds. The experimentally obtained statistical A of the wrinkles determined by AFM is in very close agreement with the theoretical A_{cal} calculated from the surface modulus from Equation (2). The tiny deviation from the theoretically and experimentally quantitative relationship in Equation (2) may arise from the constraints of experimental errors (such as the measurement of A and E_f) and the assumption of the dynamic cross-linked D-A adducts as an incompressible medium with an ideal Poisson's ratio ($\upsilon = 0.5$). Thus, the established linear relationship of the amplitude of the resulting wrinkle versus surface modulus of top-layer indicates that the obtained wrinkle patterns in our systems can be precisely controlled and tailored by means of the surface modulus by the simple control of the D-A reaction, which suggests the feasibility of our strategy for the fabrication of a reversible wrinkle pattern by a dynamic D-A cross-linking reaction.

Based on these experimental results, combined with the theoretical analysis, we proposed that the reversible cross-linking process of dynamic D-A reaction at the top-layer enables the feasible, simple yet reliable, regulation of the surface moduli in situ and in a reversibly tunable manner without an external physical stimulus. Therefore, it is expected that control of the D-A reaction-induced surface modulus change in the top layer can be applied to generate and regulate wrinkles in our system. The as-prepared wrinkled surface that is subjected to multiple cycles of alternate heating at different reaction temperatures exhibits highly reversible morphology as well as a transition of surface Young's modulus (**Figure 3**). As shown in Figure 3a, the characteristic A of the wrinkle decreased from 120 to 70 nm after heating to 120 °C for 5 min, and the surface became almost smooth again after further heating for 20 min. The wrinkle transition was highly reversible for at least seven cycles with no obvious degradation of wrinkle size. The amplitude of the surface wrinkle is significantly dependent on the surface modulus. During the D-A reaction to generate wrinkles, the modulus of the top layer increased from $E = 520$ MPa for $A = 52$ nm (70 °C for 1 h) to $E = 980$ MPa for $A = 120$ nm (70 °C for 4 h). In the case of erasure, the sample was heated to 120 °C for the retro-D-A reaction, and the A value of the wrinkle and the modulus of the top layer decreased after heating for 5 min to 65 nm and 570 MPa, respectively. This phenomenon can be explained well by Equation (2) because the surface modulus of the top layer is strictly regulated by the reversible D-A reaction. The mechanical modulus mismatch between the bilayers caused by the D-A cross-linking reaction gradually decreases to the equilibrium value and the wrinkles are fully relaxed when the compressive strain ε decreases to below the critical strain ε_C. With subsequent heating to 70 °C for the D-A cross-linking reaction, the erased surface would become wrinkled again. Generation and elimination of the wrinkles are the consequences of the dynamic evolution of the compressive stress field regulated by the modulus mismatch between the bilayers through the facile control of the dynamic D-A reaction. The highly cyclic evolution of the wrinkle pattern also suggests the feasibility of our strategy for formation of a reversible wrinkle pattern based on the D-A reaction.

The highly reversible nature of the dynamic D-A reaction allows self-healing of the wrinkle pattern (**Figure 4**). As shown in Figure 4a, the wrinkled surface was first damaged by scratching with a spindle probe. After heating to 120 °C for 20 min, the surface became flat and wrinkle-free (Figure 4b). Heating at 70 °C for 4 h resulted in an intact and identically sized wrinkle pattern once again (Figure 4c). This result indicates that the wrinkle pattern induced by the D-A reaction

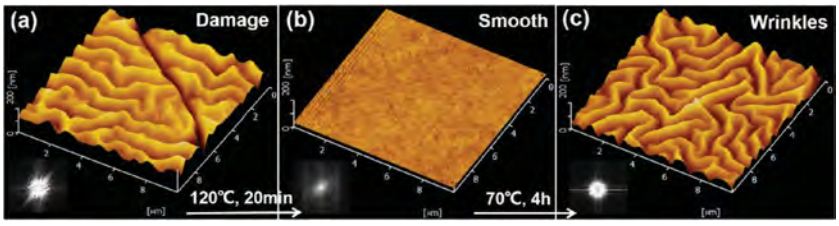

Figure 4. 3D AFM images illustrating the as-prepared wrinkle pattern a) fabricated at 70 °C for 4 h and then damaged by a spindle probe, b) subsequent heating at 120 °C for 20 min to erase the damaged pattern to a wrinkle-free smooth plane, c) followed by heating at 70 °C for 4 h to recover the wrinkle pattern. The insets at the left bottom show the FFT results from the corresponding AFM images. The thickness of the top layer is approximately 105 nm.

exhibits self-healing by an in situ thermal operation due to the dynamic pattern that is regulated by a dynamic chemical reaction.

The reversible wrinkle pattern controlled by the dynamic D-A reaction can serve well for the development of a new type of smart materials that can change their physical properties, e.g., surfaces with tunable optical, adhesion, and wettability properties, by dynamically tuning surface geometry in response to external stimuli. Firstly, the adhesion force of the wrinkled surface is measured by using force-mode AFM. The experimental values of the pull-off force are extracted from the minimum of the retraction curves and are taken as the adhesion force.[45–47] The characteristic force-displacement curves were obtained for a sequence of wrinkled surfaces fabricated at 70 °C for different durations and subsequently erased at 120 °C (Figure S9). The as-prepared wrinkled surface shows clear pull-off events and increasing adhesive force from the original 540 (red line) to 922 nN (amaranthine line). After heating to 120 °C for 20 min, a clear drop in the pull-off force was observed, which indicates that the film shows a decrease of adhesion force when the surface morphology changes from the wrinkled to wrinkle-free state. With increasing wrinkle size, the adhesion forces of the wrinkled surface are enhanced. The adhesive and nonadhesive states were reversibly cycled by the control of the D-A reaction by switching the heating (**Figure 5**a), which demonstrates the feasibility of the highly tunable adhesion. The adhesion force of the wrinkled patterns can be switched for more than five cycles, during which the adhesion force does not fluctuate significantly.

The wettability properties of the wrinkled surface were also investigated by means of contact angle measurements. Figure 5b presents the changes in water contact angle (WCA) and surface free energy measured at various stages of the D-A and retro-D-A reactions over six cycles. The WCA shows a dramatic increase from the initial value of 53° to 120° with heating at 70 °C for the D-A reaction. After heating to 120 °C for 20 min, the WCA decreased to the original value of 52°. The dramatic cyclical change of the surface free energy from approximately 52.8 to 24.7 mN m^{-1} can be attributed to the appearance and erasure of surface microarchitecture that is controlled by the D-A reaction (Figures 5b and S10,11). Surface chemistry and morphology are the two key factors that govern the wettability of a surface.[48–50] Upon heating to the D-A reaction temperature, the gradual generation of the patterns leads to a large increase in surface roughness, which greatly changes the wettability of the surface and significantly improves the contact angle. The change of surface materials from soft mixtures to cross-linked polymer might further improve the contact angle. Thus, the increased contact angles and decreased surface energy are due to both the surface wrinkle morphology and the top-layer's properties. The retro-D-A reaction, with a de-cross-linking process, restores the initial state of the surface materials and modulus, which leads to the erasure of wrinkle pattern and the restoration of the surface wettability to its original value. This result indicates that the wettability of our wrinkled surface can be tuned dynamically by controlling the surface modulus and cross-linking density under a facile thermal process of the dynamic D-A reaction.

Furthermore, the reversible wrinkle pattern can enable the capacity for switchable optical behavior. Figure 5c presents

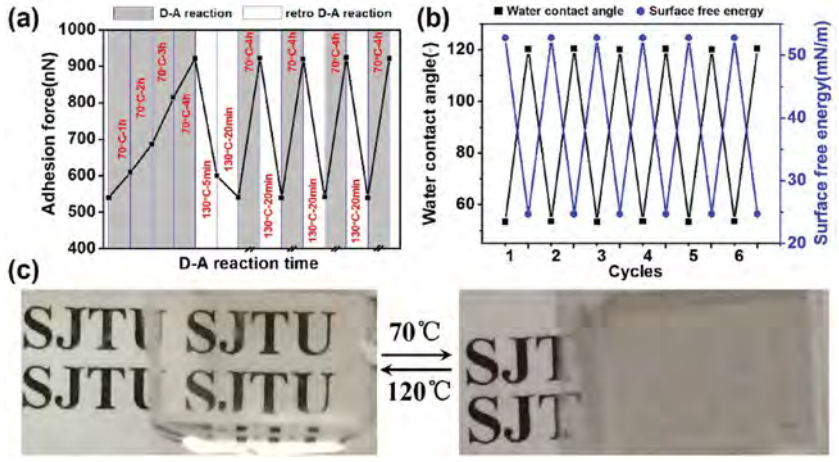

Figure 5. a) Changes in the adhesion force measured on the reversible wrinkled surface with sequential, cyclic control of the D-A reaction at 70 °C and subsequent retro D-A reaction at 120 °C. The gray and white regions represent the ongoing D-A reaction (heating at 70 °C) and the retro-D-A reaction (heating at the higher temperature of 120 °C), respectively. The inset texts depict the reaction temperature and time. The thickness of the top layer is approximately 75 nm. b) Changes in water contact angle (black line, left vertical axis) and surface free energy (blue line, right vertical axis) of on the reversible wrinkled surface with sequential, cyclic control of the D-A reaction at 70 °C and subsequent retro D-A reaction at 120 °C. The black square and blue circle represent water contact angle and surface free energy, respectively. The thickness of the top layer is approximately 75 nm. c) Optical images of the reversible wrinkled surface overlaying "SJTU" printed paper demonstrate the reversible switching capability of transmittance between optically transparent (left) and opaque (right) that correspond to wrinkled pattern and wrinkle-free state of the film. These states are acheived by sequential, cyclic thermo-control heating at 70 °C for 24 h and then heating at a higher temperature of 120 °C for 20 min, respectively. The thickness of the top layer is approximately 200 nm.

a representative result of switchable optical transparency in the wrinkled and wrinkle-free states of our reversible wrinkle system that undergoes sequential, cyclic heating to 70 °C for 24 h and then 120 °C for 20 min, respectively. The as-prepared wrinkled surface was opaque with a frosted glasslike appearance, and the covered "SJTU" could not be observed. The opacity is due to the extensive scattering of light by the micro/nanoscale surface structures (Figure S12).[11,12] As the sheet was heated to 120 °C for 20 min to eliminate the wrinkle pattern, it became transparent and showed a clear transmitted image as a result of the absence of the wrinkles. In this way, we can prepare a ten centimeter sample with reversible transparency, which might be used as a smart window (Figure S13). Because of the simple operation and reversible characteristics of our method, a dynamic no-ink display of the slogan "AM" was also demonstrated (Figure S14). After heating at 70 °C, the "AM" regions coated with FBA/BMI became opaque and displayed "AM", due to the presence of the wrinkle pattern. The "AM" can be concealed and emerge dynamically and circularly as the wrinkle pattern is erased and rewritten by means of temperature control.

We demonstrated a facile and robust strategy for the fabrication of a reversible wrinkle pattern by utilizing dynamic chemistry to harness a physical mechanical instability to obtain a smart surface with highly reversible morphology and dynamically tunable properties in situ, by simply controlling a dynamic D-A chemical reaction. The generation and elimination of wrinkles are the consequence of the dynamic evolution of the compressive stress field regulated by the modulus mismatch between the bilayers through the dynamic D-A reaction between furan and maleimide. The reversible wrinkle pattern controlled by the dynamic D-A reaction allows accurate control of the adhesion, wettability, and optical properties. We believe that our strategy for the fabrication of a reversible wrinkle pattern through D-A reaction can be expanded to a general and promising method for obtaining multifunctional smart surfaces by the versatile dynamic chemistry that is responsive to various stimulus such as thermally reversible D-A reactions and carbene coupling reactions, photoresponsive cycloadditions, pH-responsive imine covalent bonds from aldehyde to amine, glucose-responsive boronic ester bonds, and so on. Thanks to the nature and versatility of dynamic chemical reactions, the resulting highly reversible wrinkled pattern can enable broad applications for smart surfaces as functional intelligent materials and devices with topographies and properties that can be in situ tuned on-demand in a dynamic chemical way.

Experimental Section

Preparation of PDMS Substrate: The PDMS elastic sheet was prepared by mixing PDMS prepolymer (Sylgard 184, Dow Corning) in a 10:1 base:curing agent ratio, followed by drop-coating on a glass slide or silicon wafer and degassing in a vacuum oven, then curing at 120 °C for 40 min (thickness approximately 400 μm).

Preparation of Wrinkle Pattern: A toluene solution of FBA and BMI (molar ratio 1:1) was spin-coated onto a PDMS sheet precast on glass substrate and then baked at 70 °C for the desired time to allow it to undergo the D-A reaction after removing residual solvent; this formed a relatively hard top-layer film on the PDMS sheet. After heating, the coated PDMS sheet was cooled to room temperature rapidly to generate the wrinkle pattern. For erasure of the wrinkle pattern, the wrinkled PDMS bilayer was heated to 120 °C (slightly above the temperature of the retro D-A reaction) and held for a duration (10–30 min) to fully eliminate the wrinkle.

Characterization: ^{1}H NMR spectra were recorded on a Varian Mercury Plus 400 MHz instrument with chloroform-d ($CDCl_3$) as the solvent and tetramethylsilane (TMS) as an internal standard at room temperature. Polymerization kinetics was traced by using a Spectrum 100 Fourier-transformation infrared absorption spectrometer (FT-IR, Nicolet IS10), which was recorded from 4000–400 cm^{-1} with a 4 cm^{-1} resolution over 32 scans. The UV–Vis absorption spectrum was recorded by using a UV-2550 spectrophotometer (Shimadzu, Japan). Average molecular weights were determined by means of gel permeation chromatography (GPC, LC-20A, Shimadzu, Japan), using tetrahydrofuran as an eluent at a flow rate of 1.0 mL min^{-1} with a combination of two columns (Shodex, KF-802 and 804, 300 × 8 mm) and equipped with a RID-10A differential refractive index detector. The sample concentration was 2 mg mL^{-1} and the injection volume was 50 μL. Observation of the surface morphology and the measurement of the top-layer film thickness were performed by using an atomic force microscope (E-Sweep, SII, Japan). For topography measurements of tapping-mode AFM, silicon tips with a radius of 10 nm, spring constant of 40 N m^{-1},and resonance frequency of 300–400 Hz were chosen. Surface line profiles were analyzed from the acquired AFM images by using digitized Nanonavi III (Seiko) offline software, and the values of amplitude and distance between two peaks of each image were statistically calculated from 20 typical wrinkle patterns. Additionally, the AFM images were subjected to 2D fast Fourier-transform (FFT) analysis to characterize the wrinkles' uniform and alignment patterns. The adhesion measurements were conducted in both contact and force modes under vacuum conditions by using silicon tips with a contact area radius of 10 nm, spring constant of 3 N m^{-1}, and resonance frequency of 60–80 Hz. The Young's modulus is calculated as the average value of the approach and the retract trace of each force curve according to the Hertz model, by using the force–distance AFM approach. Detailed information on measurement of Young's modulus by AFM can be found in our previous reports.[51,52]

Supporting Information

Supporting Information is available from the Wiley Online Library or from the author.

Acknowledgements

The authors thank the National Basic Research Program (2013CB834506) and National Nature Science Foundation of China (21274088, 51373098, and 21522403) for their financial support.

Received: April 20, 2016
Revised: June 19, 2016
Published online: August 30, 2016

[1] E. Delamarche, A. Bernard, H. Schmid, B. Michel, H. Biebuyck, *Science* **1997**, *276*, 779.
[2] M. Böltau, S. Walheim, J. Mlynek, G. Krausch, U. Steiner, *Nature* **1998**, *391*, 877.
[3] J. H. Kim, M. Yoneya, H. Yokoyama, *Nature* **2002**, *420*, 159.
[4] A. D. Stroock, G. M. Whitesides, *Acc. Chem. Res.* **2003**, *36*, 597.
[5] A. D. Campo, E. Arzt, *Chem. Rev.* **2008**, *108*, 911.
[6] A. Biswas, I. S. Bayer, A. S. Biris, T. Wang, E. Dervishi, F. Faupel, *Adv. Colloid Interface Sci.* **2012**, *170*, 2.

[7] A. Olivier, F. Meyer, J. M. Raquez, P. Damman, P. Dubois, *Prog. Polym. Sci.* **2012**, *37*, 157.
[8] Y. Engel, J. D. Schiffman, J. M. Goddard, V. M. Rotello, *Mater. Today* **2012**, *15*, 478.
[9] D. Tian, Y. Song, L. Jiang, *Chem. Soc. Rev.* **2013**, *42*, 5184.
[10] H. Jeon, S. Koo, W. M. Reese, P. Loskill, C. P. Grigoropoulos, K. E. Healy, *Nat. Mater.* **2015**, *14*, 918.
[11] H. S. Kim, A. J. Crosby, *Adv. Mater.* **2011**, *23*, 4188.
[12] S. G. Lee, D. Y. Lee, H. S. Lim, D. H. Lee, S. Lee, K. Cho, *Adv. Mater.* **2010**, *22*, 5013.
[13] Z. B. Chen, Y. Y. Kim, S. Krishnaswamy, *J. Appl. Phys.* **2012**, *112*, 124319.
[14] S. Lee, S. Kim, T. T. Kim, Y. Kim, M. Choi, S. H. Lee, J. Y. Kim, B. Min, *Adv. Mater.* **2012**, *24*, 3491.
[15] J. H. Lee, H. W. Ro, R. Huang, P. Lemaillet, T. A. Germer, C. L. Soles, C. M. Stafford, *Nano Lett.* **2012**, *12*, 5995.
[16] J. Yin, J. L. Yague, D. Eggenspieler, K. K. Gleason, M. C. Boyce, *Adv. Mater.* **2012**, *24*, 5441.
[17] D. Y. Khang, H. Jiang, Y. Huang, J. A. Rogers, *Science* **2006**, *311*, 208.
[18] S. G. Lee, H. Kim, H. H. Choi, H. Bong, Y. D. Park, W. H. Lee, K. Choi, *Adv. Mater.* **2013**, *25*, 2162.
[19] S. G. Lee, H. S. Lim, D. Y. Lee, D. Kwak, K. Cho, *Adv. Funct. Mater.* **2013**, *23*, 547.
[20] E. P. Chan, E. J. Smith, R. C. Hayward, A. J. Crosby, *Adv. Mater.* **2008**, *20*, 711.
[21] Y. Lai, F. Pan, C. Xu, H. Fuchs, L. Chi, *Adv. Mater.* **2013**, *25*, 1682.
[22] D. van den Ende, J. D. Kamminga, A. Boersma, T. Andritsch, P. G. Steeneken, *Adv. Mater.* **2013**, *25*, 3438.
[23] D. M. Drotlef, P. Blumler, A. del Campo, *Adv. Mater.* **2014**, *26*, 775.
[24] J. H. Cho, D. Datta, S. Y. Park, V. B. Shenoy, D. H. Gracias, *Nano Lett.* **2010**, *10*, 5098.
[25] A. Chen, D. K. Lieu, L. Freschauf, V. Lew, H. Sharma, J. Wang, D. Nguyen, I. Karakikes, R. J. Hajjar, A. Gopinathan, E. Botvinick, C. C. Fowlkes, R. A. Li, M. Khine, *Adv. Mater.* **2011**, *23*, 5785.
[26] C. Cao, H. F. Chan, J. Zang, K. W. Leong, X. Zhao, *Adv. Mater.* **2014**, *26*, 1763.
[27] E. Lee, M. Zhang, Y. Cho, Y. Cui, J. Van der Spiegel, N. Engheta, S. Yang, *Adv. Mater.* **2014**, *26*, 4127.
[28] C. Zong, Y. Zhao, H. Ji, X. Han, J. Xie, J. Wang, Y. Cao, S. Jiang, C. Lu, *Angew. Chem. Int. Ed.* **2016**, *55*, 3931.
[29] S. Yang, K. Khare, P.-C. Lin, *Adv. Funct. Mater.* **2010**, *20*, 2550.
[30] J. Genzer, J. Groenewold, *Soft Matter* **2006**, *2*, 310.
[31] J. Rodríguez-Hernández, *Prog. Polym. Sci.* **2015**, *42*, 1.
[32] S. Singamaneni, V. V. Tsukruk, *Soft Matter* **2010**, *6*, 5681.
[33] N. Bowden, S. Brittain, A. G. Evans, J. W. Hutchinson, G. M. Whitesides, *Nature* **1998**, *393*, 146.
[34] J. Y. Chung, A. J. Nolte, C. M. Stafford, *Adv. Mater.* **2011**, *23*, 349.
[35] Z. Wei, J. H. Yang, J. Zhou, F. Xu, M. Zrinyi, P. H. Dussault, Y. Osada, Y. M. Chen, *Chem. Soc. Rev.* **2014**, *43*, 8114.
[36] E. Trovatti, T. M. Lacerda, A. J. Carvalho, A. Gandini, *Adv. Mater.* **2015**, *27*, 2242.
[37] S. Yu, R. Zhang, Q. Wu, T. Chen, P. Sun, *Adv. Mater.* **2013**, *25*, 4912.
[38] W. Hu, Z. Ren, J. Li, E. Askounis, Z. Xie, Q. Pei, *Adv. Funct. Mater.* **2015**, *25*, 4827.
[39] A. Gandini, *Prog. Polym. Sci.* **2013**, *38*, 1.
[40] G. Rivero, L. T. T. Nguyen, X. K. Hillewaere, F. E. Du Prez, *Macromolecules* **2014**, *47*, 2010.
[41] Y. L. Liu, C. Y. Hsieh, *J. Polym. Sci. Polym. Chem.* **2006**, *44*, 905.
[42] J. Bai, H. Li, Z. Shi, J. Yin, *Macromolecules* **2015**, *48*, 3539.
[43] K. Adachi, A. K. Achimuthu, Y. Chujo, *Macromolecules* **2004**, *37*, 9793.
[44] L. M. Polgar, M. van Duin, A. A. Broekhuis, F. Picchioni, *Macromolecules* **2015**, *48*, 7096.
[45] E. Svetushkina, N. Puretskiy, L. Ionov, M. Stamm, A. Synytska, *Soft Matter* **2011**, *7*, 5691.
[46] J. Erath, S. Schmidt, A. Fery, *Soft Matter* **2010**, *6*, 1432.
[47] H.-J. Butt, B. Cappella, M. Kappl, *Surf. Sci. Rep.* **2005**, *59*, 1.
[48] G. d. Crevoisier, *Science* **1999**, *285*, 1246.
[49] M. Callies, D. Quéré, *Soft Matter* **2005**, *1*, 55.
[50] B. Xin, J. Hao, *Chem. Soc. Rev.* **2010**, *39*, 769.
[51] Y. C. Gan, J. Yin, X. S. Jiang, *J. Mater. Chem. A* **2014**, *2*, 18574.
[52] H. H. Hou, Y. C. Gan, J. Yin, X. S. Jiang, *Adv. Mater. Interfaces* **2014**, *1*, 1400385.